Comparison of fully non linear and weakly nonlinear potential flow solvers for the study of wave energy converters undergoing large amplitude of motions

Lucas Letournel, Jeffrey C. Harris, Pierre Ferrant, Aurélien Babarit, Guillaume Ducrozet, Michel Benoit, Emmanuel Dombre

Proceedings of the ASME 2014 33rd International Conference on Ocean, Offshore and Arctic Engineering
OMAE2014
June 8-13, 2014, San Francisco, California, USA

OMAE2014-23912

COMPARISON OF FULLY NONLINEAR AND WEAKLY NONLINEAR POTENTIAL FLOW SOLVERS FOR THE STUDY OF WAVE ENERGY CONVERTERS UNDERGOING LARGE AMPLITUDE MOTIONS

Lucas Letournel *
Pierre Ferrant, Aurélien Babarit, Guillaume Ducrozet
LHEEA Lab, CNRS UMR6598
Ecole Centrale Nantes
Nantes, France

Jeffrey C. Harris †
Michel Benoit, Emmanuel Dombre
Saint-Venant Hydraulics Lab
Univ. Paris-Est (EDF R&D, CEREMA, ENPC)
Chatou, France

ABSTRACT

We present a comparison between two distinct numerical codes dedicated to the study of wave energy converters. Both are developed by the authors, using a boundary element method with linear triangular elements. One model applies fully nonlinear boundary conditions in a numerical wavetank environnment (and thus referred later as NWT), whereas the second relies on a weak-scatterer approach in open-domain and can be considered a weakly nonlinear potential code (referred later as WSC). For the purposes of comparison, we limit our study to the forces on a heaving submerged sphere. Additional results for more realistic problem geometries will be presented at the conference.

INTRODUCTION

Among the marine renewable energy sources, wave energy is a promising option. Despite the great number of technologies that have been proposed, currently no wave energy converter (WEC) has proven its superiority over others and become a technological solution. Usual numerical tools for modeling and designing WECs are based on boundary elements methods in linear potential theory [1–4]. However WECs efficiency relies on large amplitude motions [5], with a design of their resonance frequencies in the wave excitation. Linear potential theory is thus inadequate to study the behavior of WEC in such configuration. CFD tools, while able to handle large amplitude motions, present a calculation time significantly too large, several hours per wave period [6, 7], to propagate incident waves or even perturbations in long term simulation with reasonable CPU cost du to their dissipative numerical schemes.

We report here on progress with two different numerical codes, fulfilling the conditions laid down by the WECs : modeling of large amplitude motion response in a reasonable calculation time. Due to the different formulations, the fully nonlinear approach (NWT) is expected to be more precise but slower than the weak-scatterer approach (WSC). A significant plus of the WSC relies on the fact that the incident wave does not need to be propagate from a wave-maker, allowing also the mesh to be refined only on the vicinity of the body. We are working towards freely moving (or constrained) floating bodies, but in this paper we limit our results to submerged bodies with prescribed motion.

The solution of potential flow with the boundary element in the context of a numerical wavetank was pioneered by Longuet-Higgins and Cokelet [8]. In their work, they used the mixed Eulerian-Lagrangian (MEL) approach, solving the Laplace equation in an Eulerian coordinate system, and then advecting the boundary mesh locations. Many more numerical wavetanks have been developed since then, in both two and three dimensions, and the issues regarding the development of such a model have been reviewed by Tanizawa [9]. More recent developments have been focused on improving three dimensional numerical wavetanks, as computational time can still be significant, and issues

*Author of correspondence for the WSC
†Author of correspondence for the NWT

of gridding, model stability, and accuracy can be problematic for complex geometries.

Here we report on comparisons between the early stages of model development for two different approaches. To allow for flexibility in gridding, for both numerical code designs, we use an unstructured triangular mesh, but with different integration techniques or boundary conditions. A global comparison of the two codes is summarized in Table 1. The development of these two codes are part of a French national project, MONACOREV [10], aiming to provide tools for the design of wave energy converters.

THEORY

We consider a fluid domain, D, under the assumptions of incompressible and inviscid fluid with irrotational motion. We can thus introduce the velocity potential ϕ, which satisfies the Laplace equation:

$$\nabla^2\phi(x,y,z,t) = 0 \tag{1}$$

in the fluid domain, D, with a boundary Γ. The Laplace equation is transformed with Green's second identity into the boundary integral equation (BIE):

$$\alpha(\mathbf{x}_l)\phi(\mathbf{x}_l) = \int_\Gamma \left[\frac{\partial\phi}{\partial n}(\mathbf{x})G(\mathbf{x},\mathbf{x}_l) - \phi(\mathbf{x})\frac{\partial G}{\partial n}(\mathbf{x},\mathbf{x}_l)\right] d\Gamma \tag{2}$$

where G is the free-space Green's function for the NWT and Rankine sources for the WSC (Weak Scatterer Code), for the Laplace equation, and α is the interior solid angle at a point. In three dimensions, for a distance $\mathbf{r} = \mathbf{x} - \mathbf{x}_l$, we have:

$$G(\mathbf{x},\mathbf{x}_l) = \frac{1}{4\pi|\mathbf{r}|} \tag{3}$$

$$\frac{\partial G}{\partial n}(\mathbf{x},\mathbf{x}_l) = -\frac{1}{4\pi}\frac{\mathbf{r}\cdot\mathbf{n}}{|\mathbf{r}|^3} \tag{4}$$

There are many variations of the boundary element method, but for NWTs nearly all use the collocation method, where the BIE is evaluated at the vertices of the mesh. See Tanizawa [9] for more details.

NWT Boundary Conditions

Along the boundaries, information is needed about the particle motion and the velocity potential, hence we require two boundary conditions.

Kinematic Free Surface Condition For the fully nonlinear approach, we consider Lagrangian time updating, tracking fluid particles from the gradient of the velocity potential:

$$\mathbf{u} = \nabla\phi \tag{5}$$

Dynamic Free Surface Condition Given the fluid velocity, we can solve for the change in velocity potential on the free surface, taking the free surface pressure to be zero:

$$\frac{D\phi}{Dt} = -gz + \frac{1}{2}\nabla\phi\cdot\nabla\phi + p \tag{6}$$

We then use the MEL approach of Longuet-Higgins and Cokelet [8].

Body Condition For a body with prescribed motion, given the motion of the center of mass, $\mathbf{x}_{body}$, and the angular velocity, ω, we then obtain at a point $\mathbf{x}$ of the body surface:

$$\frac{\partial\phi}{\partial n}(\mathbf{x}) = \left(\frac{D\mathbf{x}_{body}}{Dt} + \omega\times(\mathbf{x}-\mathbf{x}_{body})\right)\cdot\mathbf{n} \tag{7}$$

We then note that the body forces can be computed by rearranging Eq. 6 as:

$$\frac{p}{\rho} = -\phi_t - gz - \frac{1}{2}\nabla\phi\cdot\nabla\phi \tag{8}$$

Thus the forces on a body at an instant are $\mathbf{F} = \int p\mathbf{n}\,d\Gamma$.

Weak-Scatterer Approximation

The Weak-Scatterer approximation is based on the decomposition of the potential flow and the free-surface elevation (ϕ,η) into an incident (ϕ_0,η_0) and a perturbation component (ϕ_p,η_p). The second is supposed to be small compared to the first, which implies that the linearization of the free surface equations can be written on the position of the incident wave.

A semi-Lagrangian time derivative operator based on the incident velocity projected onto the vertical is defined according to the approximation as:

$$\frac{D_{0z}}{Dt} = \frac{\partial}{\partial t} + \mathbf{v}_{0z}\cdot\nabla \quad \text{with} \quad \mathbf{v}_{0z} = \frac{\partial\phi_0}{\partial z}\mathbf{z} \tag{9}$$

The free surface boundary conditions can then be put in this frame of reference:

Kinematic Free Surface Condition

$$\frac{D_{0z}\eta_p}{Dt} = -\frac{\partial \eta_0}{\partial t} - \nabla\phi \cdot \nabla\eta + \frac{\partial \phi}{\partial z} - \eta_p . \frac{\partial}{\partial z}\nabla\phi_0 \cdot \nabla\eta_0 \quad (10)$$

Dynamic Free Surface Condition

$$\frac{D_{0z}\phi_p}{Dt} = -\frac{\partial \phi_0}{\partial t} - g\eta - \frac{1}{2}\nabla\phi^2 + \frac{\partial \phi_0}{\partial z}\frac{\partial \phi_p}{\partial z} + \frac{1}{2}\eta_p \frac{\partial}{\partial z}\nabla\phi^2 \quad (11)$$

Body Condition The boundary condition on the body is similar to the fully nonlinear approach: the motion of the body is calculated at each time step and its mesh updated according to its motion. The wetted surface is thus defined with the incident wave elevation.

$$\frac{\partial \phi_p}{\partial n} = -\frac{\partial \phi_0}{\partial n} + \mathbf{V}\cdot\mathbf{n} \quad \text{on the wetted surface of the body} \quad (12)$$

The pressure is also calculated on this wetted surface with the equation (8). The time derivative of the potential on the body is solved at each time step with another BIE, based on the Lagrangian derivative of the potential.

NUMERICAL IMPLEMENTATION

NWT implementation, outside of programming issues, can be divided essentially into two parts: the solution of the BIE, and the time-updating.

Solution to the BIE

In the collocation method, the BIE, Eq. 2, is written for a series of points, $\mathbf{x}_i$, over the surface of the domain which compose a computational grid of elements, Γ_j. Using continuous linear elements, we decompose the BIE into 2 integrals, written for the element, j, and a point, l:

$$I_{\sigma,j}(\mathbf{x}) = \iint \frac{\partial \phi}{\partial n}(\mathbf{x}) G(\mathbf{x},\mathbf{x}_l) d\Gamma_j \quad (13)$$

$$I_{\mu,j}(\mathbf{x}) = \iint \phi(\mathbf{x}) \frac{\partial G(\mathbf{x},\mathbf{x}_l)}{\partial n} d\Gamma_j \quad (14)$$

This results in the final linear system of equations that we can represent as:

$$\mathbf{G}_{ij}(\phi_n)_i = \mathbf{H}_{ij}\phi_i \quad (15)$$

where the matrix **G** includes all integrals of the Green's function, and **H** includes all integrals of the normal derivative of the Green's function, as well as the α terms along the diagonal. In each case, we use the iterative method GMRES (Generalized minimal residual method) [11] for solving the resulting system of equations.

Fully Non-linear Approach

Discretization Though based on the general approach of Grilli et al. [12], by using triangular finite elements, we take a departure from this earlier NWT. We impose a local coordinate system, (ξ,η), for each element, and in these coordinates a field variable, f, (the geometry, velocity potential, and normal flux), on an element can be interpolated based on the values at the nodes:

$$f(\xi,\eta) = \sum_{j=1}^{N_{elem}} N_j(\xi_1,\xi_2) f_j \quad (16)$$

where for linear elements the shape functions N_j are simply ξ_1, ξ_2, $1-\xi_1-\xi_2$. We presently make use of linear elements, but for the fully nonlinear approach, we make use of numerical integration for non-singular integrals, to retain the capability to easily return to higher-order boundary elements, where no closed-form solutions are known. An example of such a HOBEM approach with triangular mesh is the NWT of Bai and Eatock Taylor [13].

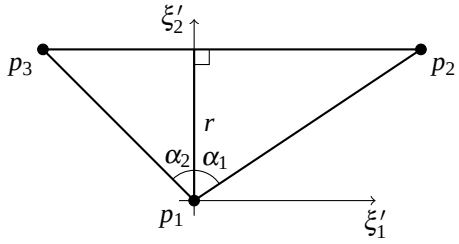

FIGURE 1: VARIABLE DEFINITIONS FOR COMPUTING SINGULAR INTEGRALS.

Singular integrals When considering one of the nodes which make up the element being integrated (or one of the respective multiple-nodes), the integral of the Green's function becomes singular. For flat elements, though, with some additional definitions (Fig. 1) the closed-form solutions are easy to derive.

Note that, as the field variables are linear in space, we can express this local integral as a linear combination of $\int\int \frac{1}{\sqrt{\xi_1'^2+\xi_2'^2}} d\xi_1' d\xi_2'$, $\int\int \frac{\xi_1'}{\sqrt{\xi_1'^2+\xi_2'^2}} d\xi_1' d\xi_2'$, and $\int\int \frac{\xi_2'}{\sqrt{\xi_1'^2+\xi_2'^2}} d\xi_1' d\xi_2'$. By using polar coordinates, transforming

(ξ_1', ξ_2') to (r', θ'), this integral becomes quite simple. For example:

$$\int\int \frac{1}{r'} dx'dy' = \int_{-\alpha_2}^{\alpha_1} \int_0^{r\sec\theta} \frac{1}{r'} r' dr' d\theta \tag{17}$$

$$= \int_{-\alpha_2}^{\alpha_1} r\sec\theta d\theta \tag{18}$$

$$= [r(\log(\cos\theta + \sin\theta) - \log(\cos\theta - \sin\theta))]_{-\alpha_2}^{\alpha_1} \tag{19}$$

Similarly,

$$\int\int \frac{x'}{r'} d\xi_1' d\xi_2' = \frac{r^2}{2\cos\alpha_2} \tag{20}$$

$$\int\int \frac{y'}{r'} d\xi_1' d\xi_2' = \frac{r^2}{2}(\log(\cos\alpha_2 + \sin\alpha_2) - \log(\cos\alpha_2 - \sin\alpha_2)) \tag{21}$$

We then need to compute r and α_1 and α_2 from the positions of the three nodes. If we set $\vec{v}_1 = \mathbf{p_2} - \mathbf{p_1}$ and $\vec{v}_2 = \mathbf{p_3} - \mathbf{p_2}$, then we can define a variable $f_{mid} = \frac{\vec{v}_1 \cdot \vec{v}_2}{\vec{v}_2 \cdot \vec{v}_2}$, so we obtain:

$$r = \sqrt{\vec{v}_2 \cdot \vec{v}_2 - f_{mid}(\vec{v}_2 \cdot \vec{v}_2)} \tag{22}$$

$$\alpha_1 = \tan^{-1} \frac{f_{mid}|\vec{v}_2|}{r} \tag{23}$$

$$\alpha_2 = \tan^{-1} \frac{(1 - f_{mid})|\vec{v}_2|}{r} \tag{24}$$

From this, it is trivial to sum the contributions of the various elements and nodes. For the other BIE type, note that since the element is flat, and the integral of the normal derivative of the Green's function is proportional to $r \cdot n$, it is zero.

Note that for higher-order elements, it is typical to use a polar coordinate transformation in combination with a cubature rule. For quadratic triangular elements this has been detailed by Eatock Taylor and Chou [14]. As well, integrals become nearly-singular when the target points are very close to the elements being considered. A typical approach is to use adaptive integration in this situation, such as that described by Grilli et al. [12]. This has not yet been tested here.

Regular integrals For regular integrals, we make use of the Dunavant [15] cubature rules:

$$\int f(\xi_1, \xi_2) d\Gamma \approx \sum w_i f(\xi_i, \eta_i) \tag{25}$$

One way to test the order of integration required is to vary the number of integration points for a simple analytic solution, as

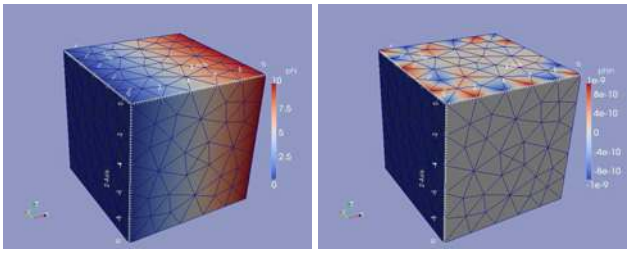

FIGURE 2: EXAMPLE BOUNDARY VALUES FOR ϕ (LEFT) AND FOR ϕ_n (RIGHT) FOR A MIXED BOUNDARY CONDITION PROBLEM WITH THE ANALYTIC SOLUTION, $\phi = x$.

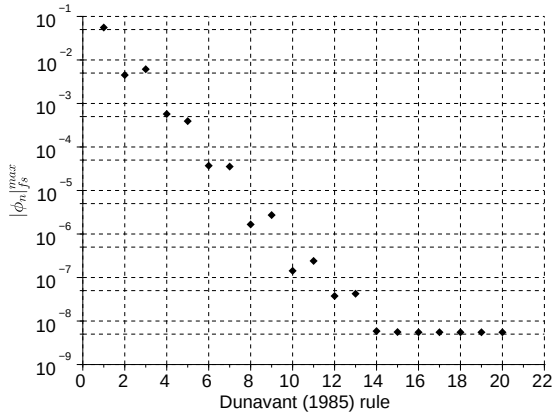

FIGURE 3: CONVERGENCE IN BOX-CASE FOR DIFFERENT DUNAVANT RULES.

in the case of Grilli and Svendsen [16]. In this case, we consider a box (Fig. 2) with a mixed Dirichlet-Neumann problem, identical to that found in real applications, but with an analytic solution, in this case $\phi = x$. We then can look at the error on the free-surface as we increase the order of integration (Fig. 3). As singular integrals are computed analytically, this is mostly a test of the numerical integration procedure. The lower limit, when the error does not improve with higher is not a limitation of the rounding error, but rather is an effect of the finite error tolerance of the linear solver, GMRES, which in this case was set to 10^{-10}.

Parallelization For accelerating the calculations, we use a parallelization approach equivalent to the 'all-pairs' approach used in N-body problems. In this case, the domain is partitioned using METIS [17], and the interaction of a single subdomain on all other points is computed by a given processor. In terms of the linear system of equations above, each processor then has stored a subset of the columns of the matrices. For simplicity, since the time-stepping and initialization are not nearly as time-consuming

as the Laplace solver, this is duplicated on all processors.

Rather than calculating the α from the geometry of the mesh, often the rigid mode method is used. If we set ϕ to be 1 everywhere, then ϕ_n is clearly 0, hence:

$$\mathbf{H}_{ij}1 = 0 \tag{26}$$

If we adjust the **H** matrix by zeroing out the diagonal:

$$\mathbf{H'}_{ij} = \begin{cases} 0 & \text{if } i = j \\ \mathbf{H'}_{ij} & \text{if } i \neq j \end{cases} \tag{27}$$

then we can easily determine:

$$\mathbf{H}_{diag} = -\mathbf{H'}_{ij}1 \tag{28}$$

We write this in terms of matrix-vector products, as opposed to the more traditional sum of off-diagonal matrix values, because the only communication between processors required in the entire NWT is a simple parallel matrix-vector multiplication.

With this albeit simple parallelization scheme, computational speed has been shown to increase by about 7.5 times on a small 8 CPU computer, for problems around 2,500 elements. More sophisticated approaches will be needed when using larger computer clusters.

Weak-scatterer Approach

Discretization Linear triangular elements is also used, via an isoparametric parameterization, describing as well the geometry as the evolution of the unknowns.

$$\begin{aligned} f(\mathbf{x}) &= f(\mathbf{x}_1) + u(f(\mathbf{x}_2) - f(\mathbf{x}_1)) + v(f(\mathbf{x}_3) - f(\mathbf{x}_1)) && (29) \\ &= f(\mathbf{x}_{cg}) + \nabla_s(f) \cdot \mathbf{x_{cg}x} && (30) \end{aligned}$$

$\mathbf{x}_{cg}$ is the center of gravity of the element $(\mathbf{x}_1\mathbf{x}_2\mathbf{x}_3)$ and $\nabla_s(f)$ represents the surface gradient of f and can be calculated with the derivatives of f along u and v.

Integral Equations The integral in the BIE (2) can be separated into two terms, depending respectively on $\frac{\partial \phi}{\partial n}$ and ϕ.

$$\left[\overline{\overline{\Delta}} \iint_{S_j} G(\mathbf{x}, \mathbf{x}_l) d\Gamma_j - \left(\oint_{C_j} \frac{\mathbf{n_j} \wedge \mathbf{dl_j}}{G(\mathbf{x}, \mathbf{x}_l)} \right) \overline{\overline{\Sigma}} \right] \cdot \begin{pmatrix} \frac{\partial \phi}{\partial n}(\mathbf{x}_1) \\ \frac{\partial \phi}{\partial n}(\mathbf{x}_2) \\ \frac{\partial \phi}{\partial n}(\mathbf{x}_3) \end{pmatrix} \tag{31}$$

$$\left[\overline{\overline{\Delta}} \iint_{S_j} \frac{\partial G(\mathbf{x}, \mathbf{x}_l)}{\partial n} d\Gamma_j - \left(\oint_{C_j} \frac{\mathbf{r} \wedge \mathbf{dl_j}}{G(\mathbf{x}, \mathbf{x}_l)} \right) \overline{\overline{\Sigma}} \right] \cdot \begin{pmatrix} \phi(\mathbf{x}_1) \\ \phi(\mathbf{x}_2) \\ \phi(\mathbf{x}_3) \end{pmatrix} \tag{32}$$

with $\overline{\overline{\Delta}} = \frac{1}{3}.\bar{I} + \mathbf{x_{cg}x}.\overline{\overline{\Sigma}}$ and $\overline{\overline{\Sigma}} \cdot \begin{pmatrix} f(\mathbf{x}_1) \\ f(\mathbf{x}_2) \\ f(\mathbf{x}_3) \end{pmatrix} = \nabla_s(f)$.

The double integrals comes from the Constant Panel discretization. Their analytical solutions were given by Guevel for AQUAPLUS [18]. The analytical solutions for the single integrals with Rankine sources were developed with a decomposition on each sides of the triangular panel. See Letournel et al. [19] for more details.

WSC Particularities A procedure using polar coordinates is also used in the WSC to analytically remove singularities. Asymptotic solutions for each integral have also been developed to speed up calculation, for distant panels from the field point.

Points at different face intersections (free-surface/body or body/body) also require a special treatment, to take into account the different conditions (Dirichlet/Neumann or different normal velocity and normal definition). The points have been doubled for each condition to apply, i.e., same location, different points and a condition in concordance with their face. The potential continuity on the intersection is enforced if needed, as is the aspect ratio of the elements with common edge at the intersections.

The two following features have been implemented to reduce calculation time by reducing the number of unknowns in the influence coefficients calculation.

Symmetry The symmetry of the domain $\mathscr{D}$ can be taken into account by decomposing it in two symmetrical parts $\mathscr{S}_1$ and $\mathscr{S}_2$. For a point M in $\mathscr{S}_1$, the BIE can be written using collocation :

$$\begin{aligned} &\phi(M)\Omega(M) + \sum_{P_1 \in \mathscr{S}_1} CD(M,P_1)\phi(M) - \sum_{P_1 \in \mathscr{S}_1} CS(M,P_1)\frac{\partial \phi}{\partial n}(M) \\ &+ \sum_{P_2 \in \mathscr{S}_2} CD(M,P_2)\phi(M) - \sum_{P_2 \in \mathscr{S}_2} CS(M,P_2)\frac{\partial \phi}{\partial n}(M) = 0 \end{aligned}$$

The symmetry, $P_2 = Sym(P_1)$, implies that $\phi(P_1) = \phi(P_2)$ and $\frac{\partial \phi(P_1)}{\partial n} = \frac{\partial \phi(P_2)}{\partial n}$. The BIE can then be written as:

$$\begin{aligned} &\phi(M)\Omega(M) + \sum_{P_1 \in \mathscr{S}_1} \left(CD(M,P_1) + CD(M,Sym(P_1))\right)\phi(M) \\ &- \sum_{P_1 \in \mathscr{S}_1} \left(CS(M,P_1) + CS(M,Sym(P_1))\right)\frac{\partial \phi}{\partial n}(M) = 0 \end{aligned}$$

The unknowns are thus reduced to the field points of $\mathscr{S}_1$. This implies a calculation time cut by two for the influence coefficients calculation and the boundary value problem solution.

Open Domain In the Open Domain approximation, the potential on the bottom and the side walls of the mesh vanishes. Only the wetted surface of the body and the free-surface are left to mesh. If the side walls and the bottom are sufficiently far away

from the body, the influence of these faces on the body and the center of the free-surface is neglected. Moreover, if the potential on the outer points of the free-surface is set to zero, the overall solution of the BVP will not be affected.

The unknowns on the bottom and the side walls can then be suppressed from the BVP, if the two following conditions are fulfilled: The dimensions of the free-surface meshed are far greater than the dimensions of the body. The potential on the outer points of the free-surface is set to zero. The side walls are still roughly meshed for the calculation of the solid angles, but the nodes on these faces have no unknowns for the resolution of the BVP.

To ensure the last condition, a numerical beach is applied on the resolution of the free-surface equations, to obtain a perturbation component gradually decreasing to zero.

A last aspect has been considered to reduce influence coefficients time calculation. Since the body is considered non-deformable, the influence coefficients of the body on itself are constant, for any motion. Moreover if the free-surface has no incident component (i.e. no incident wave is imposed), the free-surface nodes are fixed in time and their auto-influence coefficients also need only one calculation. So the only influence coefficients left to calculate at each time step are the influence from the body to the free-surface and reciprocally.

Time Integration

Fully Non-linear Approach Following the developments of Grilli et al. [12], in the tradition of Dold and Peregrine [20], we use a Taylor's series expansion to advance the free-surface variables in time, first solving:

$$\begin{aligned}
\nabla^2\phi &= 0 \\
\frac{D\mathbf{x}}{Dt} &= \mathbf{u} = \nabla\phi \\
\frac{D\phi}{Dt} &= -gz + \frac{1}{2}\nabla\phi\cdot\nabla\phi - \frac{p}{\rho}
\end{aligned}$$

and then, using the same discretization for the Laplace equation,

$$\begin{aligned}
\nabla^2\phi_t &= 0 \\
\frac{D^2\mathbf{x}}{Dt^2} &= \nabla\phi_t + \nabla(\frac{1}{2}\nabla\phi\cdot\nabla\phi) \\
\frac{D^2\phi}{Dt^2} &= -gw + \mathbf{u}\cdot\frac{D\mathbf{u}}{Dt} - \frac{1}{\rho}\frac{Dp}{Dt}
\end{aligned}$$

which is combined to obtain:

$$\begin{aligned}
\mathbf{x}(t+\Delta t) &= \mathbf{x}(t) + \Delta t\frac{D\mathbf{x}}{Dt}(t) + \frac{(\Delta t)^2}{2}\frac{D^2\mathbf{x}}{Dt^2}(t) \\
\phi(t+\Delta t) &= \phi(t) + \Delta t\frac{D\phi}{Dt}(t) + \frac{(\Delta t)^2}{2}\frac{D^2\phi}{Dt^2}(t)
\end{aligned}$$

This has the advantage of making use of ϕ_t, which is needed for computing the forces on a body anyway.

Note that this requires us to compute tangential derivatives along the free-surface. We apply a technique similar to Bai and Eatock Taylor [13], whereby the boundary conditions are computed on each finite element, and then to evaluate on a point, a weighted average is taken of the elements neighboring the node. This is effectively equivalent to a low-order center-difference scheme, extended to unstructured grids. For the second-order derivatives, linear interpolation of the velocity components on an element is used.

Wave absorption For absorption, it is typical to use an absorbing beach, first implemented by Baker et al. [21]. Some of the various approaches that have been considered previously are discussed by Cao et al. [22] and Clément and Muselet [23]. A more rigorous and modern look has been given by Kim [24], considering the dispersion relation in a damping region. Here we follow Grilli and Horrillo [25], we make use of both a numerical absorbing beach, applying a pressure on the free surface proportional to the surface flux:

$$\begin{aligned}
p_{beach} &= \nu(r,t)\frac{\partial\phi}{\partial n} \\
\nu(r,t) &= \nu_0\,(r - r_{min})^{\mu}
\end{aligned}$$

where r is the distance from the center of the NWT, r_{min} is the size of the region inside the beach, and ν_0 and μ are parameters.

Weak-scatterer Approach

Time-Marching Scheme The time marching scheme is based on the free-surface equations, modified with the weak-scatterer formulation.

$$\frac{D_{0z}\eta_p}{Dt} = -\frac{\partial\eta_0}{\partial t} - \nabla\phi\cdot\nabla\eta + \frac{\partial\phi}{\partial z} - \eta_p.\frac{\partial}{\partial z}\nabla\phi_0\cdot\nabla\eta_0 \quad (33)$$

$$\frac{D_{0z}\phi_p}{Dt} = -\frac{\partial\phi_0}{\partial t} - g\eta - \frac{1}{2}\nabla\phi^2 + \frac{\partial\phi_0}{\partial z}\frac{\partial\phi_p}{\partial z} + \frac{1}{2}\eta_p\frac{\partial}{\partial z}\nabla\phi^2 \quad (34)$$

A 4th order Runge-Kutta scheme is used for the advance in time. The Weak-Scatterer formulation implies to solve the BVP, to determine the normal velocity on the free-surface, on the three different mesh configurations during a time step : for the substep at t, $t+\frac{dt}{2}$ and at $t+dt$. However the mesh configuration is the same for the substep $t+dt$ of the time step t and the one for the substep t of the time step $t+dt$. It is then possible to reduce the number of influence coefficient calculations per time step at two, in stocking the mesh and influence coefficients of the last substep of a time step for the first substep in the next time step.

Once the normal velocity on the free-surface is determined, the spatial derivatives of η and ϕ are to be computed to solve

the free-surface equations. These are calculated using B-Splines rather than the isoparametric representation to obtain a better accuracy. Virtual nodes are to be defined around the plane of symmetry for this purpose.

If the body is intersecting the free-surface, a remeshing step is needed to mesh the wetted surface. However the body mesh can be entirely re-created since there is no information that need to be transmitted in time, except its global motion and position.

Pressure Calculations The pressure on the body is calculated according to the equation (8), and thus the time derivative of the potential is needed. This quantity is obtained by finite difference in a post-process calculation, since the body motion is forced and does not need to be computed at each time-step.

Numerical Beach The numerical beach is designed to damp the perturbation components on the outer part of the free-surface. It is a requirement for the open domain approximation, and moreover ensures that we obtain no reflection on the boundary.

The numerical beach consists in a ramp function, multiplying all the terms in the free-surface equations.

$$ramp(r) = \frac{1 - tanh\left(r^a - r_0^a\right)}{2}$$

The parameters r_0 and a adjusts respectively the mean radius and the width of the beach. Thus, in the middle of the free-surface, $ramp(r=0)=1$, and on the outer domain, $ramp(r>>r_0)=0$.

COMPARISON FOR RADIATION PROBLEM

Submerged spheres may be used as prototypes for spherical structures typical of offshore engineering, and more recently in the context of wave energy [28]. Spheres under the influence of waves have been studied for many years, both as a radiation problem, determining the forces and waves produced by heaving sphere, and as a diffraction problem, determining the forces and perturbation from a fixed sphere.

The heaving motion of the sphere generates circular waves which propagate in all directions. Ferrant [26] studied the flow generated by a body performing a large amplitude heave motion under the free surface of a perfect fluid, with a time domain code, based on Body Exact condition and linearized free-surface equations with Green functions. This case was also treated by Delhommeau [29] under linear consideration with Aquaplus. More recently, Guerber [30] presented the hydrodynamic coefficients of a heaving submerged sphere, compared to those obtained numerically with Aquaplus and analytical solutions based on linear approximation and infinite depth, by Srokosz [27].

The body in forced motion is a sphere with a radius $a = 10m$, submerged at $z_0 = -2a = -20m$ below the mean free surface elevation and moving according to a forced heaving motion. The wavelength, k and amplitude, Ar, of this motion vary and the force on the body is studied harmonically on the fundamental frequency and the 3 first harmonics.

Figure 4 presents a comparison of the linear solutions (small amplitude) given by NWT and WSC for the harmonic coefficients of the hydrodynamic effort, for the fundamental frequencies for different periods of motion, with the reference solutions of Ferrant [26], Aquaplus and Sorkosz [27]. Figures 5 and 6 show the non-linear solutions given by NWT, WSC and Ferrant.

Weak Scatterer Approach

This case, under the weak scatterer formulation, is effectively a Body-Exact approach, since the incident wave is zero. Thus, while the free surface equations are solved on the mean position of the free surface elevation, the body condition is solved on the exact position of the body. The Open Domain approximation is applied, which implies an infinite depth approximation.

Half the sphere is meshed with approximately 550 nodes for 1100 elements, with a grid spacing of $0.125a$. The free-surface is meshed circularly on 3 wave lengths, with a minimum grid spacing at the center of 1/50. The total symmetric mesh counts 1600 nodes for 3000 elements. We ran the simulation on 3 periods with 100 time steps per period. We observe a quasi-state at the end of the first period. Thus we evaluate the harmonic coefficients for the 2 latter periods. The time per iteration is close to 3 seconds. The resulting harmonic coefficients for small amplitude (Fig. 4) compare well with those from Ferrant [26].

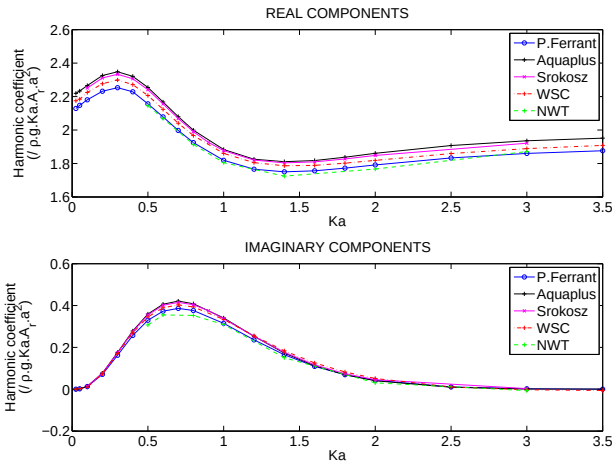

FIGURE 4: COMPARISON OF HARMONIC COEFFICIENTS COMPUTED BY WSC AND NWT FOR SMALL AMPLITUDE=0.025a., WITH AQUAPLUS, FERRANT [26] AND SROKOSZ [27] FOR REFERENCE

Fully Nonlinear Approach

For the fully-nonlinear approach, we run the same test cases, with a somewhat different grid. Not being configured for infinitely-deep water, we ensure that it is deep, with a rectangular grid 5 wavelengths across, 3 wavelengths deep, with a minimum grid spacing (at the center of the free-surface) of 1/40 of the wavelength, and a maximum grid spacing of 1/2 of the wavelength (which also falls within the absorbing beach area), stretching the grid to allow for high resolution near the center of the domain. The sphere is meshed with a grid spacing of $0.2a$. The grid is created with Gmsh [31], using the frontal method, with a varying number of elements (depending on the test), but approximately 1300 nodes and 2400 elements. Time-step is adaptive, setting the CFL condition to 0.5, and each timestep takes approximately 19 CPU-seconds. While this is considerably slower than the WSC for a slightly smaller number of elements, as this code is parallelized, for any given application on a multi-core or distributed memory system, the two perform similarly. The use of a finite depth, and setting the time-step by the CFL condition, results in a larger number of timesteps per simulation – in this case, about 1000 timesteps for a case of $ka = 1.0$, with an increasing number of timesteps for smaller ka values. On 12 processors, then, it takes about 27 minutes to run such a test. To perform comparatively better, it will be necessary to consider higher-order elements in the future, as is now common, which could provide more accuracy for a given number of elements, and with integrals that do not have a closed-form solution.

We see that for the third and fourth harmonics, there are significant differences between the NWT and the other results. It is unclear whether this is due to the nonlinear terms, or whether this is the beginning of some numerical instability or inaccuracy. Further convergence tests will be required to verify this.

DISCUSSION AND SUMMARY

We see above that both codes give a good agreement of the hydrodynamic coefficients fo a submerged sphere (Figs. 5 and 6). While not a particularly challenging problem, and ignoring viscous effects which could be important, it shows that the two models produce results which match expectations, and begin to show the differences and respective advantages of the two methods, given the types of improvements being added to each.

For the fully nonlinear NWT, we are working on moving past simple parallelization and integrating the BEM solver with a working fast multipole method implementation, and using higher-order elements, which will take advantage of the flexibility offered by using numerical integration.

In contrast, we have applied symmetry and other simplifications of the mathematical problem with the weakly nonlinear approach. It is also faster here, for a moderate number of elements, which is an expected result from making use of analytic computations of the influence coefficients. While the use of analytic integrals makes extension to the use of higher-order elements or fast multipole method difficult, this weakly nonlinear approach has the added advantage of easily prescribing complex, large amplitude incident waves.

As the respective models are developed and improved, we are working on validation cases for surface-piercing bodies. Test cases with wavemakers, including validation of wave generation and absorption, as well as more complex and realistic problem geometries, will be presented at the conference.

ACKNOWLEDGMENT

The authors would like to thank the French ANR (Agence Nationale de la Recherche) for their financial support of this work as a part of the project ANR11-MONU-018-01 MONACOREV.

REFERENCES

[1] Falcão, A., 2007. "Modelling and control of oscillating-body wave energy converters with hydraulic power take-off and gas accumulator". *Ocean Engng.*, ***34***, pp. 2021–2032.

TABLE 1: COMPARISON OF METHODS IN EACH NUMERICAL MODEL.

Model	NWT	WSC
Boundary conditions	Fully nonlinear	Weakly nonlinear
Singular integrals	Analytic	Analytic [19]
Regular integrals	Numerical (Dunavant 1985)	Analytic [19]
Time integration	2nd-order Taylor's series	4th-order Runge-Kutta
Geometry	Linear triangular	Linear triangular
Approx. time (per timestep)	19 CPU-s	3 CPU-s
Parallelized	Yes	No
Symmetry	No	Yes
Infinite depth	No	Yes

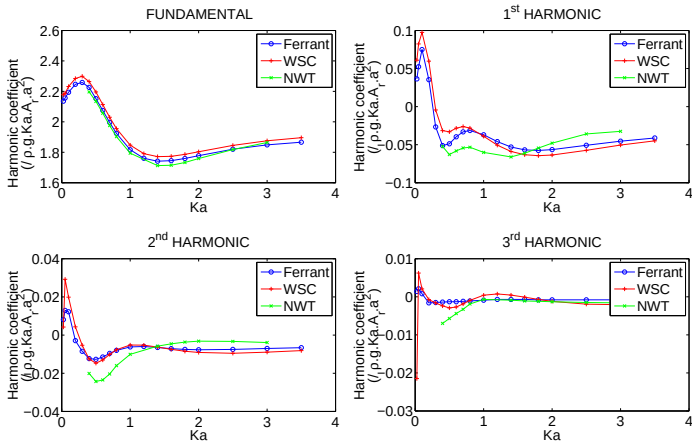

(a) REAL COEFFICIENTS, AMPLITUDE=0.3a

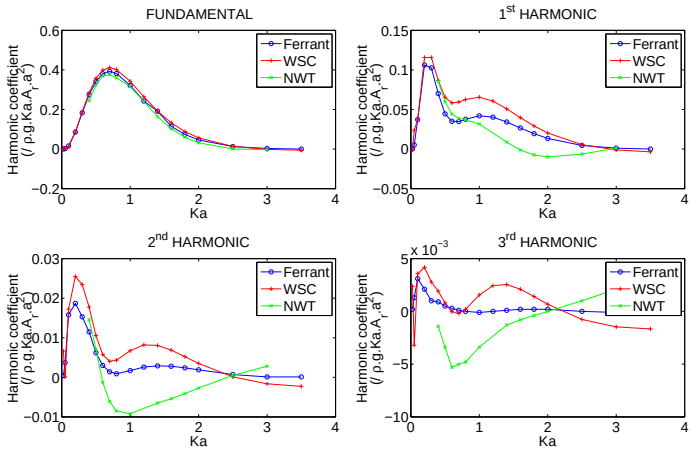

(b) IMAGINARY COEFFICIENTS, AMPLITUDE=0.3a

FIGURE 5: COMPARISON BETWEEN WSC AND NWT FOR AN AMPLITUDE OF 0.3 TIMES THE RADIUS OF THE SPHERE.

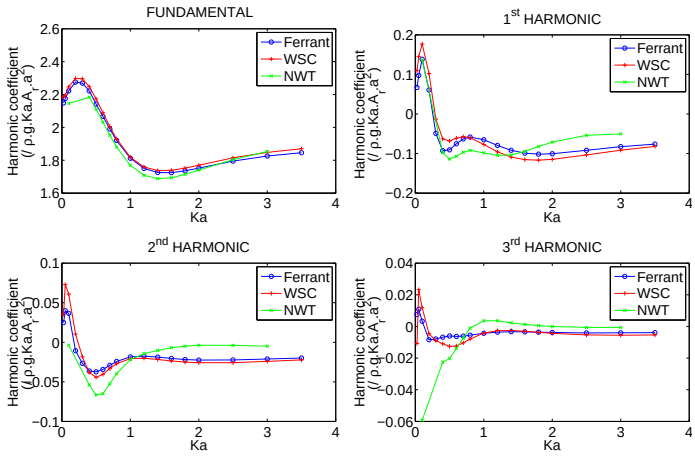

(a) REAL COEFFICIENTS, AMPLITUDE=0.5a

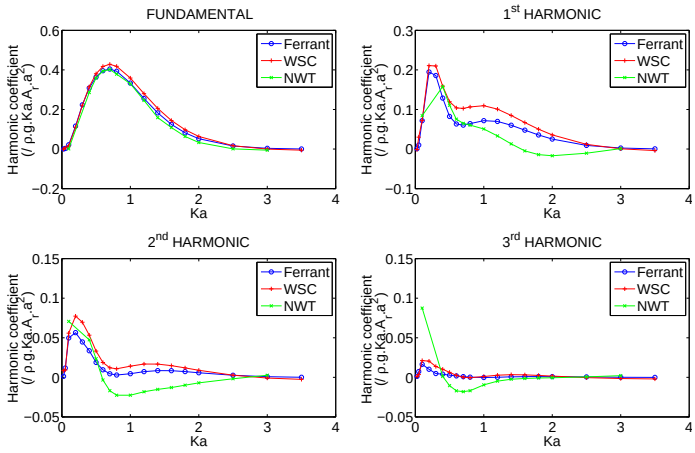

(b) IMAGINARY COEFFICIENTS, AMPLITUDE=0.5a

FIGURE 6: COMPARISON BETWEEN WSC AND NWT FOR AN AMPLITUDE OF 0.5 TIMES THE RADIUS OF THE SPHERE.

[2] Ricci, P., Saulnier, J., Antonio, F., and Pontes, M., 2008. "Time domain models and wave energy converters performance assessment". In ASME 27th Intl. Conf. on Offshore Mech. and Artic Engng.

[3] McCabe, A. P., 2004. "An Appraisal of a Range of Fluid Modelling Software". *Supergen Marine Workpackage*, ***2***(October).

[4] Folley, M., Whittaker, T. W. T., and Hoff, J. V., 2007. "The design of small seabed-mounted bottom-hinged wave energy converters". In 7th EWTEC.

[5] Falnes, J., 2000. *Ocean Waves and Oscillating Systems: Linear interaction including wave energy extraction.* Cambridge University Press.

[6] Luquet, R., 2007. "Simulation numérique de l'écoulement visqueux autour d'un navire soumis à une houle quelconque". PhD thesis, École Centrale de Nantes.

[7] Bhinder, M. A., Mingham, C. G., Causon, D. M., Rahmati, M. T., Aggidis, G. A., and Chaplin, R. V., 2009. "A joint numerical and experimental study of a surging point absorbing wave energy converter". In 28th Intl. Conf. Ocean, Offshore and Artic Engng., pp. 1–7.

[8] Longuet-Higgins, M. S., and Cokelet, E., 1976. "The deformation of steep surface waves on water, I. A numerical method of computation". *Proc. Royal Society A,* ***350***, pp. 1–26.

[9] Tanizawa, K., 2000. "The state of the art on numerical wave

tank". In Proceeding of 4th Osaka Colloquium on Seakeeping Performance of Ships, pp. 95–114.

[10] MONACOREV, 2012. http://lheea.ec-nantes.fr/doku.php/monacorev.

[11] Saad, Y., and Schultz, M. H., 1986. "GMRES: a generalized minimum residual algorithm for solving nonsymmetric linear systems". *SIAM J. Sci. Comp.*, ***7***, pp. 856–869.

[12] Grilli, S. T., Guyenne, P., and Dias, F., 2001. "A fully nonlinear model for three-dimensional overturning waves over arbitrary bottom". *Intl. J. Num. Methods in Fluids*, ***35***, pp. 829–867.

[13] Bai, W., and Taylor, R. E., 2006. "Higher-order boundary element simulation of fully nonlinear wave radiation by oscillating vertical cylinders". *Appl. Ocean Res.*, ***28***, pp. 247–265.

[14] Taylor, R. E., and Chau, F. P., 1992. "Wave diffraction theory – some developments in linear and nonlinear theory". *J. Offshore Mech. and Arctic Engng.*, ***114***, pp. 185–194.

[15] Dunavant, D. A., 1985. "High degree efficient symmetrical Gaussian quadrature rules for the triangle". *Intl. J. Num. Methods Engng.*, ***21***, pp. 1129–1148.

[16] Grilli, S. T., and Svendsen, I. A., 1990. "Corner problems and global accuracy in the boundary element solution of nonlinear wave flows". *Engng. Anal. Bound. Elem.*, ***7***, pp. 178–195.

[17] Karypis, G., and Kumar, V., 1999. "A fast and high quality multilevel scheme for partitioning irregular graphs". *SIAM*, ***20***, pp. 359–392.

[18] Guevel, P., 1976. *Corps solide animé d'un mouvement quelconque dans un fluide illimité*. ENSM. 76 pp.

[19] Letournel, L., Ferrant, P., Babarit, A., and Ducrozet, G., 2012. "Développement d'un outil de simulation numérique bas sur l'approche weak-scatterer pour l'étude des systèmes houlomoteurs en grands mouvements". In Proc. of the 13th Journées de l'Hydrodynamique. Chatou, France.

[20] Dold, J. W., and Peregrine, D. H., 1984. "Steep unsteady water waves: an efficient computational scheme". In Proc. Intl. Conf. of Coastal Engng., pp. 955–967.

[21] Baker, G. R., Meiron, D. I., and Orszag, S. A., 1982. "Generalized vortex methods for free-surface flow problems". *J. Fluid Mech.*, ***123***, pp. 477–501.

[22] Cao, Y., Beck, R. F., and Schultz, W. W., 1993. "An absorbing beach for numerical simulations of nonlinear waves in a wave tank". In Proceedings of the 8th IWWWFB.

[23] Clément, A., and Muselet, C., 1996. "A differential method for the modelling of wave transmission, reflection and absorption by "numerical beaches"". In Proc. 11th IWWWFB.

[24] Kim, Y., 2003. "Artificial damping in water wave problems II: application to wave absorption". *International Journal of Offshore and Polar Engineering*, ***13***, pp. 94–98.

[25] Grilli, S. T., and Horrillo, J., 1997. "Generation and absoption of fully nonlinear periodic waves". *Journal of Engineering Mechanics*, ***123***, pp. 1060–1069.

[26] Ferrant, P., 1991. "A coupled time and frequency approach for nonlinear wave radiation". In 18th Symp. Naval Hydro.

[27] Srokosz, M. A., 1979. "The submerged sphere as an absorber of wave power". *J. Fluid Mech.*, ***95***, pp. 717–741.

[28] Mann, L. D., Burns, A. R., and Ottaviano, M. E., 2007. "CETO: a carbon free wave power energy provider of the future". In Proc. 7th EWTEC.

[29] Delhommeau, G., 1993. "Seakeeping codes Aquadyn and Aquaplus". In 19th WEGMENT School, Numerical Simulation of Hydrodynamics : Ship and Offshore Structures.

[30] Guerber, E., 2011. "Modélisation numérique des interactions non-linéaires entre vagues et structures immergées, appliquée à la simulation de systèmes houlomoteurs". PhD thesis, Université Paris-Est.

[31] Geuzaine, C., and Remacle, J.-F., 2009. "Gmsh: a three-dimensional finite element mesh generator with built-in pre- and post-processing facilities". *Intl. J. Num. Methods Engng.*, ***79***, pp. 1309–1331.